Unexpected long-range transport of glyoxal and formaldehyde observed from the Copernicus Sentinel-5 Precursor satellite during the 2018 Canadian wildfires

Leonardo M. A. Alvarado[1], Andreas Richter[1], Mihalis Vrekoussis[1,2,4], Andreas Hilboll[1], Anna B. Kalisz Hedegaard[3,1], Oliver Schneising[1], and John P. Burrows[1]

[1]Institute of Environmental Physics (IUP), University of Bremen, Bremen, Germany
[2]Center of Marine Environmental Sciences (MARUM), University of Bremen, Bremen, Germany
[3]Institute of Atmospheric Physics, German Aerospace Center (DLR), Oberpfaffenhofen-Wessling, Germany
[4]Energy, Environment, and Water Research Center, The Cyprus Institute, Nicosia, Cyprus

Correspondence to: Leonardo M. A. Alvarado (lalvarado@iup.physik.uni-bremen.de)

Abstract. Glyoxal (CHO.CHO) and formaldehyde (HCHO) are intermediate products in the tropospheric oxidation of the majority of Volatile Organic Compounds (VOC). CHO.CHO is also a precursor of secondary organic aerosol (SOA) in the atmosphere. CHO.CHO and HCHO are released from biogenic, anthropogenic, and pyrogenic sources. CHO.CHO and HCHO tropospheric lifetimes are typically considered to be short during the daytime at mid-latitudes (e.g. several hours), as they are rapidly removed from the atmosphere by their photolysis, oxidation by OH, and uptake on particles or deposition. At night and at high latitudes, tropospheric lifetimes increase to many hours or even days. Previous studies demonstrated that CHO.CHO and HCHO vertical column densities, VCDs, are well retrieved from space-borne observations using the differential optical absorption spectroscopy, DOAS. In this study, we present CHO.CHO and HCHO VCDs retrieved from measurements of the TROPOMI instrument, launched on the Sentinel-5 Precursor (S5P) platform in October 2017. We observe strongly elevated amounts of CHO.CHO and HCHO during the 2018 fire season in British Columbia, Canada, where a large number of fires occurred in August. CHO.CHO and HCHO plumes from individual fire hot-spots are observed in air masses travelling over distances of up to 1500 km, i.e. much longer than expected for the relatively short tropospheric lifetime expected for CHO.CHO and HCHO. Comparison with simulations by the particle dispersion model FLEXPART indicates that effective lifetimes of 20 hours and more are needed to explain the observations of CHO.CHO and HCHO if they decay in an effective first order process. FLEXPART used in the study calculates accurately the transport. In addition an exponential decay, in our case assumed to be photochemical, of a species along the trajectory is added. We have used this simple approach to test our assumption that the CHO.CHO and HCHO are created in the fires and then decay at a constant rate in the plume, as it is transported. This is clearly not the case and we infer that CHOCHO and HCHO are either efficiently recycled during transport, or continuously formed from the oxidation of longer-lived precursors present in the plume, or possibly a mixture of both. We consider the best explanation of the observed CHO.CHO and HCHO VCD in the

plumes of the fire is that they are produced by oxidation of longer-lived precursors, also released by the fire and present in the plume.

1 Introduction

Formaldehyde (HCHO) is produced in the oxidation of both methane (CH_4) and other Volatile Organic Compounds (VOC). Glyoxal (CHO.CHO) is the smallest alpha-dicarbonyl formed in the oxidation of many VOC containing two or more carbon atoms. Although both CHO.CHO and HCHO, which are known as OVOC (Oxygenated Volatile Organic Compounds) have similar rates of reaction with the hydroxyl radical (OH) in the troposphere, the photolysis frequency of HCHO, which absorbs and is photolysed in the ultraviolet-A (UV-A), is significantly smaller than that of CHO.CHO, which absorbs in the blue. As a result, the atmospheric lifetime of HCHO is longer than that of CHO.CHO (Atkinson, 2000). Both species are short-lived during daytime due to their rapid removal by photolysis and reaction with OH radicals (Atkinson, 2000; Volkamer et al., 2007). These processes are the major sinks of CHO.CHO and HCHO, contributing about 69% and 96%, respectively. The remaining part of HCHO is removed by deposition (4%), while for CHO.CHO, 22% are removed by SOA formation and 8% by deposition (Stavrakou et al., 2009a, c). Additionally, HCHO and probably also CHO.CHO during the night are removed by reaction with nitrate (NO_3) radicals (Atkinson, 2000). CHO.CHO and HCHO play a key role in tropospheric chemistry because they act as temporary reservoirs releasing carbon monoxide (CO) and HOx (OH and Hydroperoxyl, HO_2) free radicals, which participate in catalytic cycles creating and destroying tropospheric ozone (O_3).

The slant and vertical column densities of HCHO were first observed from space using measurements from the GOME instrument (e.g. Burrows et al., 1999, and references therein). These columns were later used to estimate the emission strength of precursor VOC (Palmer et al., 2003; Abbot et al., 2003). The simultaneous observation of CHO.CHO and HCHO (Wittrock et al., 2006) enabled an improved assessment of atmospheric VOC levels and the knowledge of the ratio of CHO.CHO-to-HCHO (R_{GF}), (Vrekoussis et al., 2010), provides some differentiation of source types. Studies have used HCHO, partly in combination with CHO.CHO to estimate the biogenic isoprene emissions (Fu et al., 2007; Stavrakou et al., 2009a, b, c; Liu et al., 2012; Marais et al., 2012). This is the largest natural source of CHO.CHO (Guenther et al., 2006; Fu et al., 2007). The amount of biogenically emitted VOC depends on several factors including, amongst others, the plant species and weather conditions (e.g. temperature and humidity) (Guenther et al., 2000). In urban and rural regions, there are also contributions to the amounts of CHO.CHO from human activities, such as from fossil fuel production, distribution and combustion: the largest anthropogenic source of VOC precursors of CHO.CHO being motor vehicle emissions due to either evaporation or incomplete combustion of fuel (Kansal, 2009). Globally, 55% of CHO.CHO is produced by biogenic precursors, while 27% are from anthropogenic and the remaining 18% from pyrogenic emissions (Stavrakou et al., 2009a). Fires and vehicle exhausts are thought to be the only two sources, which directly emit CHO.CHO (Stavrakou et al., 2009a; Zhang et al., 2016).

In August 2018, unusually high temperatures caused severe drought in some areas of North America and resulted in the outbreak of many wildfires: the province of British Columbia (BC) in Canada was one of the most affected areas. The 2018 season is the worst on record, with 6826 fires being detected and an area of approximately 22500 km^2 of land burned (Natural Resources Canada, 2018). These fires emitted many different pollutants into the atmosphere, e.g. CO, NOx, VOC, OVOC, O_3, SO_2, CO_2, HCHO, HONO, $CH_3CO.O_2.NO_2$ (PAN) and other toxic species as well as aerosols (Urbanski et al., 2018). During the transport of plumes from fires, photochemical transformation of emitted species occurs. Overall, polluted air is transported to regions where the plumes are dispersed. CHO.CHO and HCHO column amounts are observed by remote sensing from satellite using Differential Optical Absorption Spectroscopy (DOAS) on measurements of the radiances backscattered from the Earth's surface and atmosphere. The global maps of CHO.CHO and HCHO retrieved from SCIAMACHY, GOME-2, and OMI show enhanced CHO.CHO and HCHO over tropical rain forests but also over other regions with high isoprene emissions. In addition, hot-spots of CHO.CHO and HCHO from fire emissions can be detected over large wildfires (Wittrock et al., 2006; Vrekoussis et al., 2009, 2010; Lerot et al., 2010; Chan Miller et al., 2014; Alvarado et al., 2014; De Smedt et al., 2008, 2012, 2015, 2018).

In this study, we present novel observations of CHO.CHO and HCHO retrieved from the high spatial resolution observations of the instrument TROPOMI on board the S5P platform. On 7 August 2018, strongly elevated amounts of CHO.CHO and HCHO were observed over British Columbia and attributed to being predominantly from fires. Surprisingly, these elevated levels of CHO.CHO and HCHO were not limited to the vicinity of the fires. The fire plumes, which contain both CHO.CHO and HCHO remain visible for several days and appear to travel long distances from the sources. We have used forward simulations of atmospheric transport of air masses calculated using the FLEXPART model (Pisso et al., 2019). The simulations include an effective first order loss, which determines the mean effective lifetime of the tracer. Those tracers emitted over the fire hot-spots with long effective lifetimes reproduce best the evolution of the plumes of CHO.CHO and HCHO for most of the fire events, and thus provide estimates of the effective lifetimes of CHO.CHO and HCHO in the plumes, as is described in the sections below. The R_{GF} provides knowledge about their sources in the plume. CO and nitrogen dioxide, NO_2, have respectively longer and shorter lifetimes with respect to reaction with OH, and smoke and aerosol are also transported in the plumes from fires. Consequently the retrieved vertical column densities of CO and NO_2 from the TROPOMI instrument and true color images from VIIRS instrument on NPP, which measures near simultaneously with TROPOMI are used as complementary information in our interpretation of the apparent enhanced lifetime of CHO.CHO and HCHO in the plume.

2 Methods

2.1 CHO.CHO and HCHO observations

The Differential Optical Absorption Spectroscopy (DOAS) method has been successfully applied to retrieve atmospheric columns of trace gases having fingerprint narrow absorption bands in the solar spectral range from space-borne instruments (e.g. Burrows et al., 1999). As noted above, there are several studies describing retrievals of OVOC and their use for the identification of VOC sources and their emissions (Burrows et al., 1999; Palmer et al., 2001; Wittrock et al., 2006; Kurosu et al., 2007; Vrekoussis et al., 2009, 2010; Lerot et al., 2010; De Smedt et al., 2008, 2012, 2015, 2018; Hewson et al., 2013; González Abad et al., 2015; Chan Miller et al., 2014; Alvarado et al., 2014, 2015). Algorithms for the retrieval of HCHO and CHO.CHO have been developed for measurements from the SCanning Imaging Absorption spectroMeter for Atmospheric CHartographY (SCIAMACHY) (Burrows et al., 1995; Bovensmann et al., 1999), the Ozone Monitoring Instrument (OMI) (Levelt et al., 2006), and the second Global Ozone Monitoring Experiment on MetOp–A and –B (GOME2–A and–B) (Munro et al., 2016), which in combination provide a continuous dataset covering a period of more than 20 years. In this study, measurements from the TROPOMI instrument on board the Sentinel-5 Precursor (Veefkind et al., 2012) are used to retrieve atmospheric column amounts of CHO.CHO and HCHO. A brief instrument description and relevant details of the retrieval of CHO.CHO and HCHO are given below.

2.2 The TROPOMI instrument

The TROPOspheric Monitoring Instrument (TROPOMI) onboard the Copernicus Sentinal-5 Precursor satellite was launched on 13 October 2017. It has a spectral range in the UV-VIS-NIR-SWIR covering wavelengths from 270 to 500 nm in the UV-VIS, from 675 to 775 nm in the NIR and in a SWIR band from 2305 to 2385 nm. These bands allow the observation of several relevant atmospheric species, including CHO.CHO, HCHO, NO_2 and CO. TROPOMI provides nearly global coverage each day at a spatial resolution which in August 2018 was 3.5 km×7 km (7 km×7 km in the SWIR). The equator crossing time is 13:30 LT (ascending node). Similar to OMI, TROPOMI is a nadir-viewing imaging spectrograph, employing a two-dimensional CCD, one dimension collecting the spectral information, the other being used for the spatial information. The TROPOMI instrument on board the S5P satellite provides data since November 2017 (Veefkind et al., 2012).

2.3 CHO.CHO retrieval from TROPOMI measurements

In recent years, several improvements on the retrieval of CHO.CHO have been reported. In 2014, Chan Miller et al. (2014) and Alvarado et al. (2014) presented new CHO.CHO retrieval algorithms applied to OMI measurements. These studies, similar to previous studies on GOME–2A data, introduced approaches to reduce interference by other absorbers, such as liquid water and nitrogen dioxide (NO_2). In this study, an optimized retrieval algorithm for CHO.CHO was developed,

building on the heritage from the OMI CHO.CHO retrieval presented by Alvarado et al. (2014), extended and applied to S5P measurements. Previous studies have shown that cross-correlations between references cross-sections, as well as instrumental structures and shifts in the wavelength calibration can introduce systematic errors in the retrieval. As a result, a strong dependence on the fitting window was identified in the retrieved CHO.CHO slant column densities, SCDs (Chan Miller et al., 2014; Alvarado et al., 2014). In this study, a fitting window from 433 to 465 nm was chosen, which is slightly larger than windows used in previous investigations (Vrekoussis et al., 2010; Alvarado et al., 2014). This fitting window, which enables the liquid water absorption to be retrieved, leads to a reduction in the number of negative CHO.CHO SCDs over oceanic regions in comparison to a shorter fitting window (e.g. 434–458 nm), as well as a reduction in the residuals. The wavelength range selected covers the strong absorption bands of CHO.CHO (452-457 nm), which have already been used in the past to retrieve CHO.CHO from ground and ship-based DOAS configurations as well as from satellites (Sinreich et al., 2007, 2010; Wittrock et al., 2006; Vrekoussis et al., 2009, 2010; Lerot et al., 2010; Chan Miller et al., 2014; Alvarado et al., 2014). In order to optimize the quality of the retrievals, a row-dependent daily mean Pacific spectrum from the region 50°S, 160°E – 50°N, 135°W is used as a background spectrum (Alvarado, 2016), which is computed by averaging over the whole latitude range (50°S – 50°N) for each across-track viewing direction independently. In addition, the mean CHO.CHO SCD over the region 30°S, 150°W – 30°N, 150°E is computed each day and subtracted from all SCDs to correct for possible offsets. A summary of the selected absorption cross-sections, and other parameters used in the retrieval, as well as a list of the species included in the retrieval, is shown in Table 1.

SCDs depend on observation geometry. VCDs are derived from the SCDs by use of so-called air mass factors (AMFs), which depend on the trace gas profile, surface albedo, aerosols, clouds, and on solar zenith angle and measurement geometry. As the focus of this study is the observation of CHO.CHO in biomass burning emissions, a simple CHO.CHO profile with a Gaussian distribution having its maximum peak at the altitude of the aerosol layer is used (see Figure 1-A). This is based on the assumption that CHO.CHO is found at the same location as the main plume of aerosol and other trace gases. The altitude of the aerosol layer was estimated from profiles retrieved by the Cloud-Aerosol Lidar and Infrared Pathfinder Satellite Observation (CALIPSO) (Vaughan et al., 2004) (Figure 1-B). These aerosol extinction coefficients (k_{ext}) profiles retrieved at 532 nm are also used in the calculation of the AMFs by the radiative transfer model SCIATRAN (Rozanov et al., 2013). The computations have been performed on a daily basis, assuming a single scattering albedo of 0.92 and a homogenous distribution of aerosols characterized by the mean profile in the whole region of study. The latter is computed from the average of all aerosol profiles taken over the region after removing cloud-contaminated pixels (see Figure 1-C). Clouds are not explicitly accounted for in the CHO.CHO and HCHO retrievals but data are filtered for the presence of clouds using an intensity criterion corresponding to a cloud radiance fraction of about 50%.

Table 1. Summary of retrieval parameters of CHO.CHO and HCHO from S5P with the respective absorption cross-sections used.

Parameters	**Formaldehyde (HCHO)**	**Glyoxal (CHO.CHO)**
Fitting window	323.5-361 nm	433-465 nm
Polynomial	5 coefficients	5 coefficients
Cross-sections used:		
HCHO (Meller and Mootgat, 2000)	Yes (298 K)	No
CHO.CHO (Volkamer et al., 2005)	No	Yes (296 K)
NO_2 (Vandaele et al., 1998)	Yes (220 K)	Yes (220K, 2294 K)
O_4 (Thalman et at., 2013)	Yes (293K)	Yes (293 K)
O_3 (Serduchenko et al., 2014)	Yes (223 K, 243 K)	Yes (223 K)
BrO (Fleischmann et al., 2004)	Yes (223 K)	No
H_2O (Rothman et al., 2013)	No	Yes (296 K)
Liquid water (Mason et al., 2016)	No	Yes (280 K)
Ring effect	Ring cross section calculated by SCIATRAN model (Vountas et al., 1998)	
Non-linear ozone absorption effects, 2 pseudo absorption cross-sections ($O_3 * \lambda + (O_3)^2$) from Taylor expansion (Puķīte et al., 2010)	Yes	No
Iterative spike removal (Richter et al., 2011)	Applied	
Intensity offset correction	Linear offset (I/I0)	
Background spectrum	Pacific region (50° N, 135° W – 50° S, 160°)	

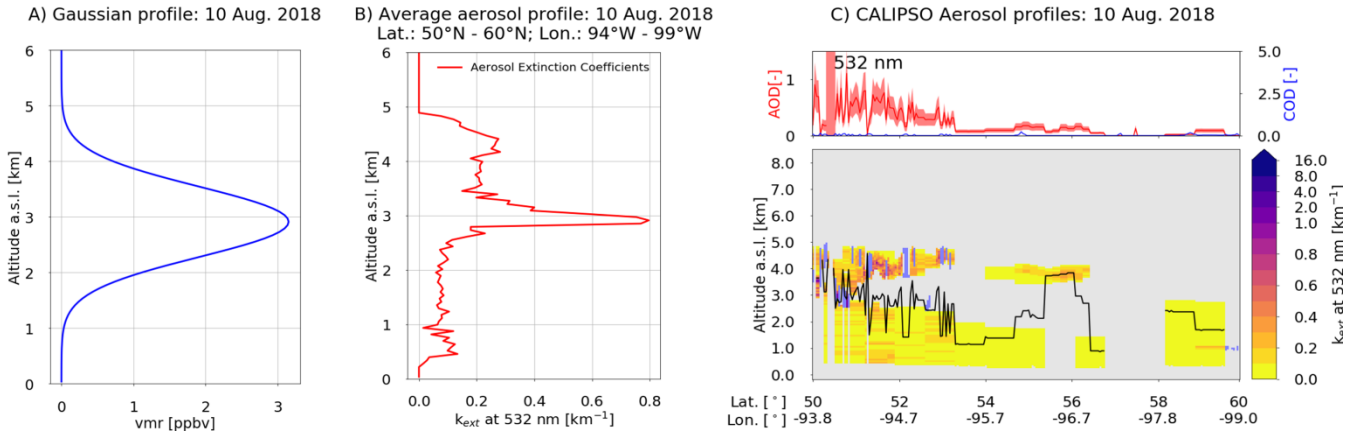

155 **Figure 1. A) CHO.CHO and HCHO profiles assumed in the computation of AMFs. B) CALIPSO profile of aerosol extinction coefficients (k_{ext}), averaged over for all latitudes and longitudes of Figure 1-C, excluding cloudy scenes. C) Top panel: Example of CALIPSO Aerosol profile extinction coefficients retrieved at a wavelength of 532 nm. Aerosol and cloud optical depth are shown as a function of latitude and longitude for every single profile. Bottom panel: Colour coded k_{ext} for every latitude and longitude in the selected region. Purple spots represent cloudy scenes. The black line depicts the aerosol layer height.**

160 **2.4 HCHO retrieval from TROPOMI measurements**

The accuracy of DOAS retrievals of HCHO is limited by cross-correlations with strong absorbers in the UV (e.g. O_3) and the signal to noise ratio of the radiance spectra measured by the instrument. Here, an updated and optimized version of the formaldehyde retrieval developed by Wittrock et al. (2006) and Vrekoussis et al. (2010) is used, which applies a slightly larger fitting window extending from 323.5 nm to 361 nm, resulting in a reduction in the noise of the retrieved slant column
165 densities. At wavelengths shorter than 336 nm, interference with O_3 is observed due to the small optical depth of HCHO, which is about three orders of magnitude smaller. This effect is compensated by applying the method described by Pukīte et al. (2010), which consists of adding two additional pseudo-cross-sections to the fit ($\lambda\sigma_{O3}$ and σ^2_{O3}) (Pukīte et al., 2010; De Smedt et al., 2008, 2015, 2018). The cross-sections of interfering species are included in the fit as listed in Table 1. In a manner similar to the retrieval of CHO.CHO, a synthetic ring spectrum (Vountas et al., 1998) is used to account for the Ring
170 effect and a row-dependent daily mean Pacific spectrum from the region 50°S, 135°W – 50°N, 160°E is used as background spectrum. A latitude dependent offset correction based on SCDs from longitudes between 180° E and 160° E is applied to the data. As for CHO.CHO, VCDs are computed using AMFs, assuming a Gaussian shape for the distribution of HCHO at the layer where the aerosols are located in the plume. Figures 2-A and 2-B show examples of CHO.CHO and HCHO fit results for 10 August 2018, compared to the differential reference cross-section for a single measurement. For an individual
175 CHO.CHO measurement, the detection limit is of the order of 5×10^{14} molec.cm^{-2}, which is about 10 times smaller than the columns detected from emissions of the wildfires over the British Columbia region of Canada. For HCHO, the detection

limit is an order of magnitude higher (4.5×10^{15} molec.cm^{-2}). The detection limit of a single S5P measurement in this study has been estimated in a manner similar to that explained in Alvarado et al. (2004).

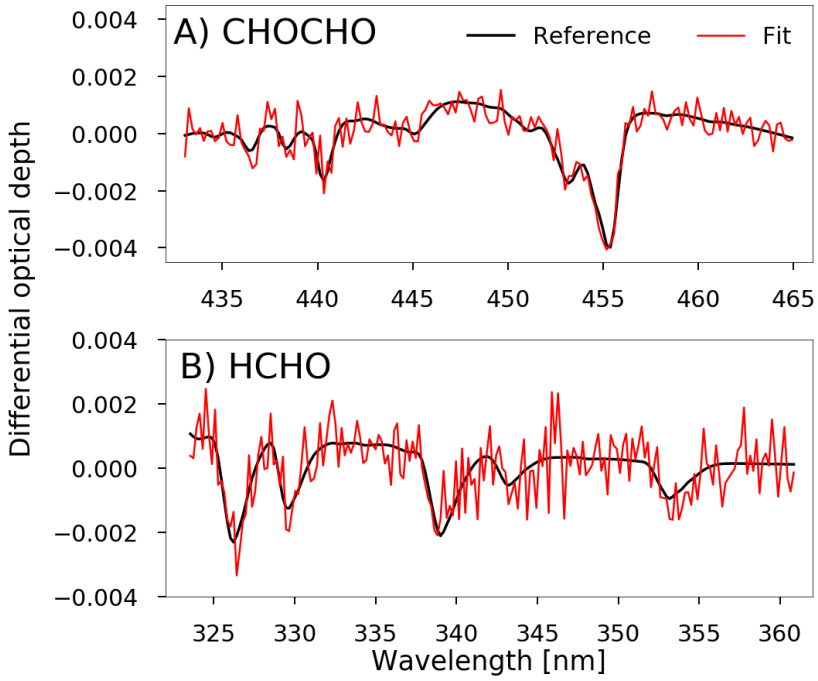

Figure 2. A) Example fit for CHO.CHO from a single measurement of S5P taken at latitude 53.0° and longitude 125.6°W, on 10 August 2018 and for a solar zenith angle of 39.3°. B) Example fit for HCHO from a single measurement of S5P taken at latitude 59.1° and longitude 109.0° W, on 10 August 2018 and for a solar zenith angle of 44.6°. The black line depicts the scaled differential cross-section and the red line the fit. The SCD values for this example are 9.3×10^{15} molec.cm^{-2} for CHO.CHO and 4.6×10^{16} molec.cm^{-2} for HCHO, respectively. The detection limit for a single measurement from S5P is estimated to be 5.0×10^{14} molec.cm^{-2} and 4.5×10^{15} molec.cm^{-2} for CHO.CHO and HCHO, respectively.

2.5 Simulation of tracer transport with FLEXPART

In order to simulate the transport of emissions from the Canadian wildfires, forward simulations with version 10.3 of the FLEXible PARTicle dispersion model FLEXPART (Stohl et al., 2005; Pisso et al., 2019) have been performed. The model was driven by using hourly wind fields from the ECMWF ERA5 reanalysis (C3S) at 0.25° horizontal resolution. As a transport model, FLEXPART does not simulate the complete set of chemical transformations leading to the observed lifetimes of trace gases in the biomass burning plumes. However, performing simulations for tracers having different mean lifetimes yields a valuable piece of information in order to understand the observed plume evolution. An effective mean lifetime can be estimated by comparing the observed behaviour of the CHO.CHO and HCHO with FLEXPART simulations of different assumed tracer lifetimes.

In FLEXPART, the effective mean lifetime τ of an emitted tracer is treated as exponential decay with a given half-life ($t_{0.5}$); τ can then be calculated according to $\tau = t_{0.5}/\ln(2)$. As part of this study, FLEXPART simulations were carried out with half-life times of 2, 4, 6, 8, 10, 12, 14, 16, 18, and 20 hours, corresponding to effective mean lifetimes of ~2.9, 5.8, 8.7, 11.5, 14.4, 17.3, 20.2, 23.1, 26.0, and 28.9 hours, respectively. As emission rates from wildfires are highly uncertain, the emission fluxes from the Canadian wildfires are assumed to be proportional to fire radiative power (FRP, see below for more details). The emissions, prescribed in the model, are taken from the Global Fire Assimilation System (GFAS) daily FRP and plume height data (Rémy et al., 2017). Simulations were performed on a daily basis for the period 6 to 23 August 2018. For each day, all fires from the GFAS data, which had an FRP of more than 3 $W.cm^{-2}$ were gridded to a 0.350° horizontal pattern. The model was then run forward in time for 120 hours, releasing the tracer for the first 24 hours (the full UTC day) from each of the 0.350° grid cells, assuming no temporal variation throughout the day. Vertically, the emissions within the grid cells were evenly distributed over the range of mean altitude of maximum injection heights given by the GFAS data for the respective grid cell. The output of the simulation contains gridded mass concentrations for each time step. Here, a grid with a horizontal resolution of 0.03125° was chosen, to match the resolution of the gridded satellite observations. Hourly output from the simulation was recorded and then vertically integrated to yield simulated tracer columns. In a post-processing step, for one specific mean lifetime, all simulation results (i.e., simulations for all fires on all days) were aggregated into one dataset. While the absolute tracer column density from the model output cannot be simply compared to the measurements, a comparison of the plume patterns and relative distribution between satellite observation and model output gives an indication about the meaningfulness of the prescribed mean lifetime. At this point, the aggregated model output for one effective mean lifetime consists of hourly latitude-longitude grids of vertical tracer columns throughout the whole study period. For comparison to the satellite observations, the hourly time slice closest to the time of overpass at 53°N was chosen.

3 Results and discussion

During August 2018, a high-temperature anomaly led to the outbreak of many fires in the Canadian Western province of British Columbia, resulting in the emission of large quantities of particles and traces gases that in turn affected air quality in the region. As shown in Figure 3-A and -B, the monthly average of CHO.CHO and HCHO vertical columns from S5P show strongly enhanced values over the fire region, suggesting that these fires were a large direct and/or indirect source of CHO.CHO and HCHO. Surprisingly, the CHO.CHO and HCHO enhancements are not limited to the main fire region but extend over large parts of Canada, where only a few fires were observed. In order to investigate the sources of CHO.CHO and HCHO and their distributions, 24-hour assimilation data of fire radiative power from the Global Fire Assimilation System (Kaiser et al., 2012) are analysed. Briefly, FRP is a measure of outgoing radiant heat from fires, measured in units of $W.cm^{-2}$ and retrieved from space by the MODerate resolution Imaging Spectroradiometers (MODIS) on board of Terra and Aqua satellites (Justice et al., 2002). The assimilated FRP spatially aggregates all valid fire and non-fire observations from

both MODIS instruments onto a horizontal resolution of 0.1° x 0.1° and computes the total FRP sums for each grid bin (Justice et al., 2002). The FRP is also used as input in the FLEXPART simulation as described in section 2.5 as a proxy for emission strength. Figure 3-C shows a monthly average FRP map over North America for August 2018.

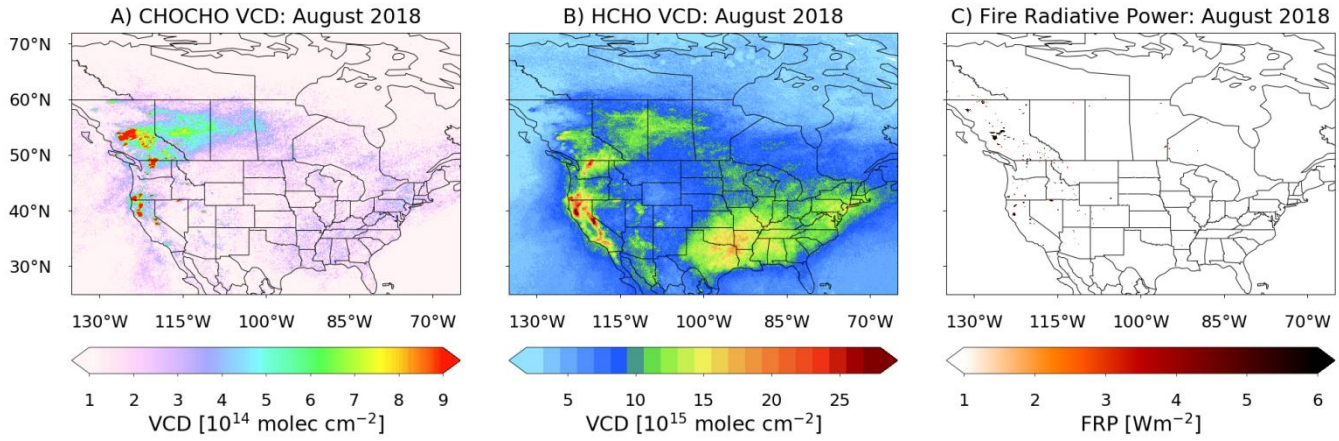

Figure 3. Monthly average of CHO.CHO (panel A) and HCHO (panel B) VCDs retrieved from the TROPOMI instrument on S5P for August 2018, and over North America (A and B). Panel C shows the integrated FRP from MODIS for the same period.

The highest CHO.CHO VCD values are found over the locations of the most intense fires, as intuitively expected. The HCHO distribution over the fire regions is similar to that of CHO.CHO, but with some differences in the relative distribution. In addition, enhanced CHO.CHO and HCHO columns are also apparent over the south-eastern US, where large isoprene emissions occur. CHO.CHO and HCHO are also detected in plumes crossing central and eastern Canada, where no fires are identified in the FRP map. This pattern is best explained by the transport of CHO.CHO and HCHO emanating from the wildfires. However, CHO.CHO and HCHO have been reported to have short atmospheric lifetimes of about ~2.2 and ~4.0 hours during daytime, respectively (Atkinson, 2000; Volkamer et al., 2005a). Assuming that the lifetime in the plume is similar to that observed at the ground, we expect that CHO.CHO would be removed reasonably close to the fire sources. HCHO would be transported further but we would also expect that it would be transported no more than approximately twice as far as CHO.CHO.

Earlier studies by Wittrock et al. (2006) and Vrekoussis et al. (2009, 2010) showed that CHO.CHO is also observed over oceanic regions, where no CHO.CHO source is expected. The potential of a) a long-range transport of CHO.CHO and/or of CHO.CHO precursors from continental areas, and b) having an unknown oceanic CHO.CHO source were discussed as a possible explanation in part of these observations, but no firm conclusions could be drawn so far. In the present study, with the support of the simulations using FLEXPART, evidence of long-range transport of CHO.CHO and HCHO or its

precursors from biomass burning emissions is investigated. In this context the transport of CHO.CHO and HCHO during two fire plume episodes form different periods (07-10 and 20-21 August 2018) are discussed below.

3.1 CHO.CHO and HCHO emissions from the British Columbia wildfires: 07-10 and 20-21 August 2018

Figure 4-A shows daily maps of CHO.CHO and HCHO VCDs over Canada for the period 7 to 10 August 2018. The most intense wildfires are found on 7 August 2018 and remain detectable until 10 August 2018. Both CHO.CHO and HCHO plumes are detected on the first day of the fire. The CHO.CHO and HCHO distributions then change from day to day. However, a large plume is clearly visible on 10 August 2018. Enhanced CHO.CHO and HCHO columns are found at a distance of up to ~1500 km from the fires, indicating transport over long distances.

To investigate possible transport pathways, forward simulations of the atmospheric transport with FLEXPART were calculated for the period when CHO.CHO and HCHO plumes are observed (see Figure 4-B), assuming an effective lifetime of 14.4 hours. The latter is significantly longer than lifetimes of CHO.CHO and HCHO found in the literature. On the other hand, the simulated pattern of air masses follows the same distinctive path as CHO.CHO and HCHO VCDs. The tracer simulated with FLEXPART spreads over the same area as CHO.CHO, providing evidence for the transport of CHO.CHO and HCHO and their precursors over continental Canada. This is more evident for the second period of interest in this study, which extends from the 20 to 21 of August 2018 (see Figure 7). While the spatial match of plume and model is good in this example, it is clear from the figure that an effective lifetime of 14.4 hours does not describe fully the extent of CHO.CHO and HCHO transported. Using shorter effective lifetimes for CHO.CHO and HCHO, taken form the literature would not reproduce the observations. However both lifetimes depend on conditions in the plume: on the diurnal photolysis and OH diurnal cycles as well as on wet/dry deposition processes and other oxidants. Consequently, comparisons of FLEXPART simulations with different effective lifetimes were performed for two selected days, as is shown in Section 3.2.

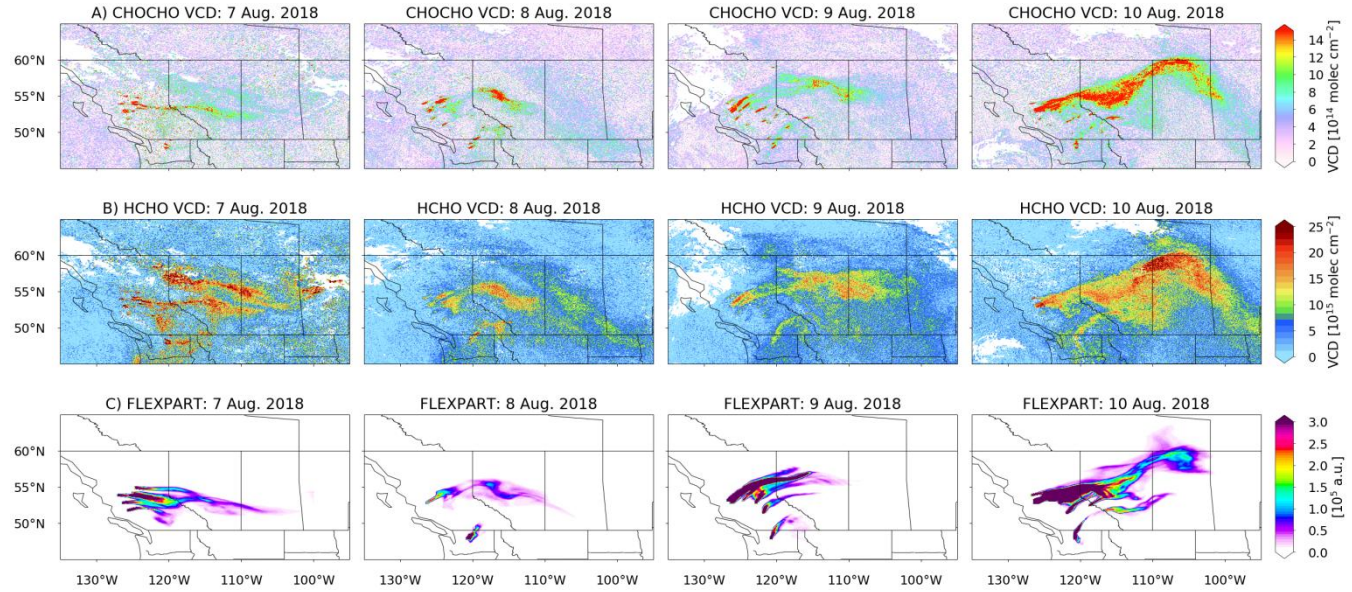

Figure 4. A) and B) Daily CHO.CHO and HCHO VCDs retrieved from S5P measurements for the period 7 to 10 August 2018. C) Distribution of a tracer with a lifetime of 14.4 hours simulated with FLEXPART for the same period. The CHO.CHO in the plume decreases on average from $3x10^{15}$ molec.cm^{-2} to $3x10^{14}$ molec.cm^{-2}, while the HCHO has a different variation in the plume but at the end of the plume, it decreases from $3x10^{16}$ molec.cm^{-2} to $1x10^{16}$ molec.cm^{-2}. The FLEXPART tracer column decreases from $3x10^{6}$ to $0.3x10^{6}$ for this specific effective lifetime of 14.4 hours.

3.2 Effective lifetimes of CHO.CHO and HCHO in the plume

Figure 5 shows the results of FLEXPART simulations assuming effective lifetimes for a surrogate chemical species of ~2.9, 14.4, 23.1, and 28.9 hours for 10 and 20 August 2018. From this figure, it is clear that only for the simulations having effective lifetimes of 23.1 hours or more, a significant fraction of the tracer emitted is present at the end of the plume as observed in the measurements. This is also illustrated in Figure 6, depicting CHO.CHO and HCHO maps for 10 August 2018. On top of these maps, contour lines are shown for the simulated air masses assuming effective lifetimes of ~2.9, 14.4, and 28.9 hours. It is evident that in both cases the tracer distributions simulated with longer effective lifetimes better describe the observed distribution of CHO.CHO and HCHO.

Figures 7-A, -B, -C present a second comparison of daily maps of CHO.CHO and HCHO VCDs with a FLEXPART tracer having an effective lifetime of 28.9 hours for 20 and 21 August 2018. It is evident that again, the tracer follows the distribution of CHO.CHO and HCHO observations, similar to the first period studied (see Figure 4). However, on 20 and 21 August 2018, the CHO.CHO and HCHO plumes spread over the ocean, where no sources are expected, up to the point at which the plume disperses after being transported over a distance of about ~600 km from the fires.

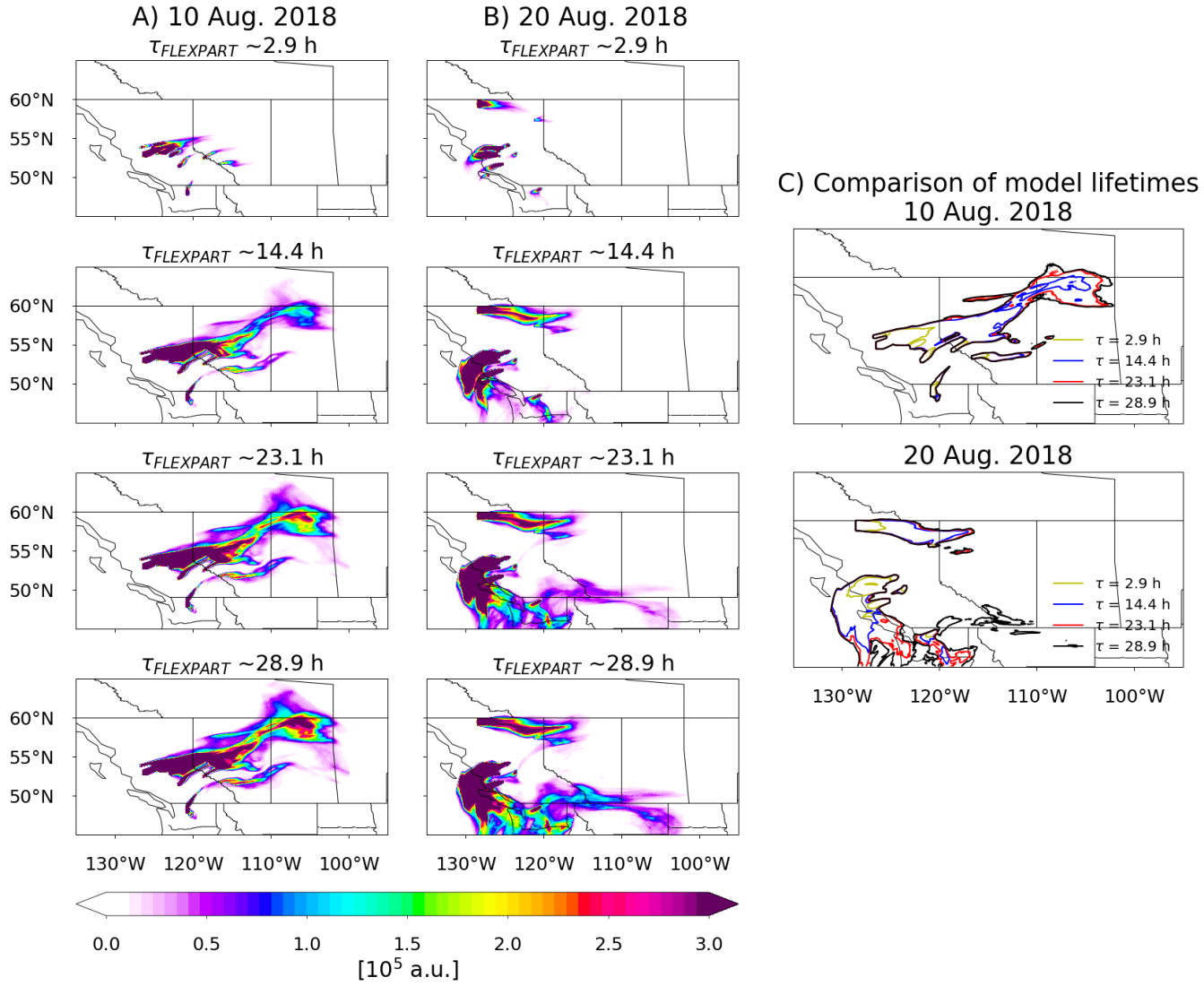

Figure 5. Daily maps of air masses simulated with FLEXPART for 10 and 20 August 2018 are shown (A and B) for selected effective lifetimes (~2.9, 14.4, 23.1, 28.9 hours). C) Contour plots of simulations for the same lifetimes are compared for 10 and 20 August 2018.

The observed behaviour of the CHO.CHO and HCHO plumes is in contrast with the short atmospheric lifetimes resulting from their rapid removal by photolysis and reaction with OH. In addition, CHO.CHO oligomerises and thus is a source of SOA formation (Schweitzer et al., 1998; Jang et al., 2002; Liggio et al., 2005; Kroll et al., 2005; Loeffler et al., 2006; Volkamer et al., 2007; Fu et al., 2007; Myriokefalitakis et al., 2008; Stavrakou et al., 2009b, c). The simplest explanation of the observations of CHO.CHO and HCHO is that, during the fire events, both species are transported and/or produced during

transport over long distances, resulting in an effective lifetime of about 28.9 hours. This would imply the transport of VOC precursors of CHO.CHO and HCHO.

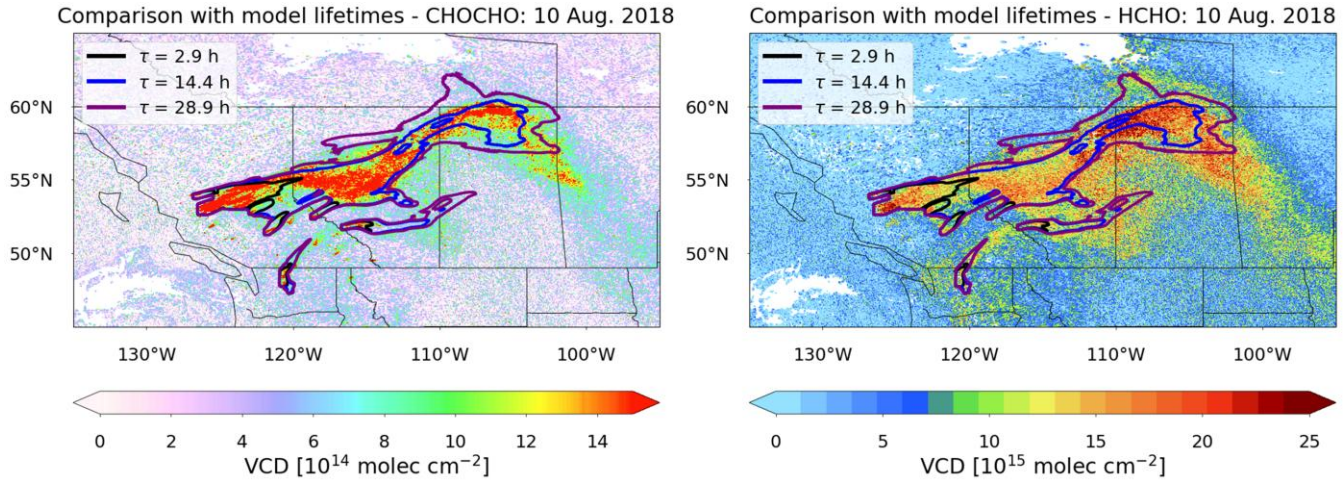

Figure 6. Daily maps CHO.CHO and HCHO VCD retrieved from S5P for 10 August 2018 compared with FLEXPART tracer simulations having three different lifetimes (~2.9, 14.4 , and 28.9 hours).

One reason for the longer range transport of the CHO.CHO and HCHO plumes is the injection of the biomass burning emissions into the free troposphere, where high wind speeds favour transport over long distances. This is a well-known effect that has also been observed for NO_2 in GOME-2 data (Zien et al., 2014). However, even at high wind speeds, the short lifetime of these species would result in much smaller dispersed plumes than the ones observed. There are three possible explanations for this apparent contradiction:

Reason 1: The lifetimes of CHO.CHO and HCHO could be significantly longer than expected in these biomass burning plumes if the OH mixing ratio and UV and visible radiation within the plume are much lower than outside the plume. There is, however, no indication that this should be the case; on the contrary, OH levels in the biomass burning plume are expected to be enhanced (Folkins et al., 1997), leading to a reduction of the expected CHO.CHO and HCHO lifetimes. In this context, it is interesting to investigate the NO_2 VCD observed. The NO_2 plumes coming from the biomass burning are shown in figure 8-B. During daytime NO_2 is removed in the gas phase by reaction with OH. Provided sufficient O_3 is present the photolysis of NO_2 produces NO and O which react respectively with O_3 to make NO_2 and oxygen molecules to make O_3. This is known as a "null cycle". NO_2 appears to decay relatively rapidly in the plumes coming from the fires. Our assumption that oxidation and photolysis of CHO.CHO and HCHO is relatively rapid, is thus not contradicted by the NO_2 decay in the fire plumes.

Reason 2: There could be an efficient recycling process between the gas and aerosol phase, resulting in the observed extended effective lifetimes of CHO.CHO and HCHO. However, this reason is considered unlikely, because there is not yet any strong evidence of HCHO being a precursor of SOA formation, and as the shape of the plumes for both trace gases is similar, a similar mechanism is expected for both. Also, evidence for the release of CHO.CHO following the formation of oligomers in the aerosol phase, is limited (Kroll et al., 2005, and references therein).

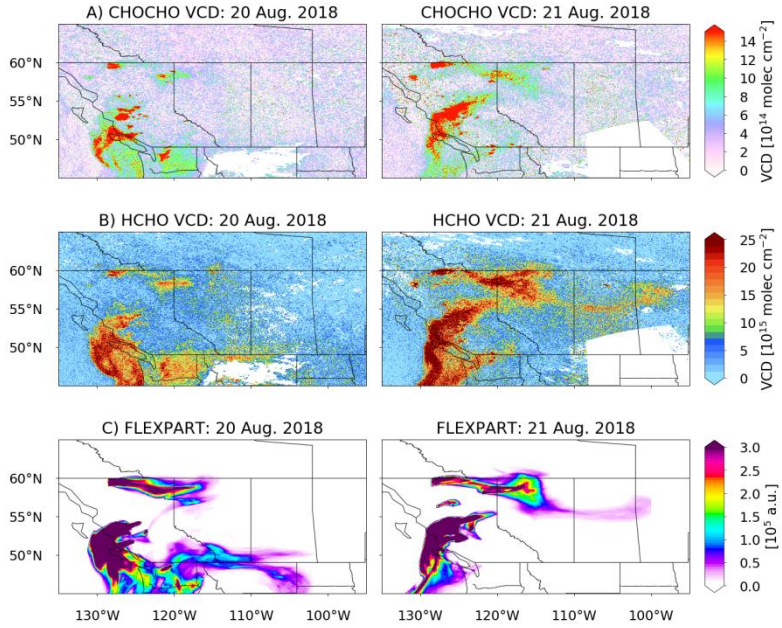

Figure 7. A) and B) Daily CHO.CHO and HCHO VCDs retrieved from S5P measurements for the period from 20 to 21 August 2018. C) Tracer distribution simulated with FLEXPART for the same period assuming a lifetime of 28.9 hours. Enhanced CHO.CHO columns spread over the ocean in a pattern similar to that simulated by the model tracer.

Reason 3: The plume could contain CHO.CHO and HCHO precursors, i.e. VOCs, which are slowly oxidized, releasing CHO.CHO and HCHO along the trajectory. If true, this would result in an apparent increase in lifetime. In order to better assess the CHO.CHO and HCHO spatial distribution seen on 10 August 2018, two additional TROPOMI retrievals have been taken into account; the column-averaged dry air mole fractions of CO, retrieved by the algorithm described in Schneising et al. (2019), and the NO_2 VCD retrieved using an algorithm similar to the one described for the GOME-2 instrument (Richter et al., 2011) and using AMF calculated following the same approach as the one described before for CHO.CHO and HCHO (see section 2.3). The CO plume shows a similar spatial pattern to those of CHO.CHO and HCHO (see Figure 8-E). As CO is a relatively long-lived tracer of fire emissions, having a lifetime with respect to OH of months, this supports the fire origin of the plume. As noted above, NO_2 is removed by OH faster than CHO.CHO and HCHO. The NO_2 VCD enhancements, in contrast to those of CHO.CHO and HCHO, are limited to the proximity of the fire hot spots (see Figure 8-D). This behaviour agrees with that assumed for a molecule with a short atmospheric lifetime. A true-colour image

from the Visible Infrared Imaging Radiometer Suite (VIIRS) clearly shows the distribution of smoke and aerosols produced because of the emission from the fires being transported and transformed (Figure 8-F). The distribution of the aerosol appears qualitatively to be similar to the CHO.CHO, HCHO, and CO distributions. We infer that the transported plumes are mixtures of CO, CHO.CHO, HCHO, aerosol and presumably other pollutants released by the fire. It is interesting to note that CHO.CHO and CO follow mainly the main plume, while the HCHO distribution is more diffuse and shows enhanced values also over regions where a thinner aerosol plume is visible in the VIIRS image. This may possibly originate from other unidentified fires or another unknown source, which is not included in our FLEXPART simulations.

As additional information, the ratio of CHO.CHO-to-HCHO, R_{GF}, is presented in Figure 8-C. Larger values of R_{GF} are found close to the location of the wildfires as already reported in previous publications (Vrekoussis et al., 2010). This is an indication of enhanced primary emissions of CHO.CHO relative to those of HCHO from fires. Lower R_{GF} values are found closer to the end of the plume implying a decreasing production of CHO.CHO relative to that of HCHO during the transport of polluted air in the plume. Another potential explanation would be the mixing in of air from different origins, having lower CHO.CHO and/or higher HCHO concentrations, during the plume transport. This is however not confirmed by the observed CO behaviour, which shows a similar spatial distribution to CHO.CHO and HCHO.

The comparison of retrieved S5P columns and FLEXPART tracer simulations discussed is based on a number of simplifications. The observational conditions of the biomass burning plumes are complex, and aerosol scattering and absorption impact on the sensitivity of the retrievals. While this is taken into account by using air mass factors for elevated plumes positioned at altitudes derived from CALIPSO observations, there remains considerable uncertainty with respect to absolute values. Aerosol loading and optical properties will vary along the plume and thus will the retrieval sensitivities. This not modelled explicitly in this study. However, the differences apparent between the spatial distributions of CHO.CHO and NO_2, which are retrieved in similar spectral regions, provide evidence for the fact that measurement sensitivity does not explain the differences in the observed VCD plume patterns. Another crucial simplification is the assumption of a constant fire emissions and the proportionality of FRP and emission strength in the FLEXPART simulations. In reality, fire emissions will also depend on the type of biomass burned, the age of the fire, the time of the day and the environmental conditions, and this will have an effect on the trace gas distribution along the plume, which reflects both chemical transformation and the history of emissions. Modelling of this time-evolution is complex, if possible at all, and out of the scope of this study. However, the observation that both CHO.CHO and HCHO are present in the biomass burning plume after extended time periods and over long distances is robust and is best explained by the release of CHO.CHO and HCHO from the transformation of longer-lived precursors and/or efficient recycling processes in the plume as discussed above.

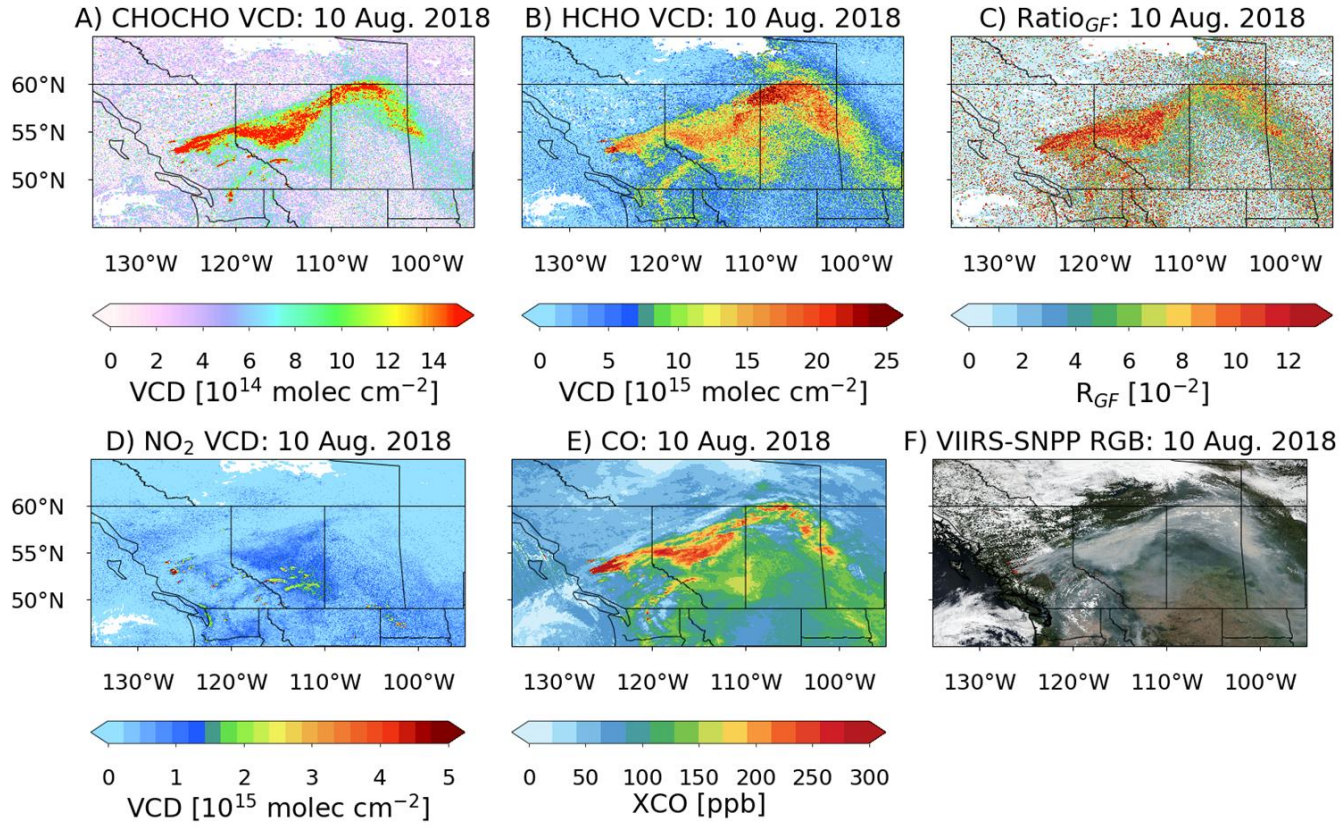

Figure 8. Panels A, B, D, and E show the CHO.CHO, HCHO, NO_2, and CO columns, respectively retrieved from S5P measurements for 10 August 2018. Note that CO columns are unfiltered and only represent a qualitative description of the plume. The AMFs used for CHO.CHO, HCHO, and NO_2 are appropriate for the biomass burning plume only. Panel C depicts the calculated CHO.CHO-to-HCHO (R_{GF}) for the same day. Panel F shows a true colour image of the aerosol distribution from VIIRS for 10 August 2018.

4 Summary and conclusions

The retrieval of CHO.CHO and HCHO VCDs from measurements of the TROPOMI instrument on board the Sentinel-5P satellite is reported. This will extend the datasets already available from the SCIAMACHY, GOME-2, and OMI instruments. The advantage of the high spatial resolution and low noise of TROPOMI for studying specific geophysical phenomena is well demonstrated in the features and plumes seen in the CHO.CHO, HCHO, CO, and NO_2 VCDs.

In this case study the satellite data show clear evidence for pyrogenic emissions of CHO.CHO and HCHO during the wildfire season in summer 2018 in British Columbia, Canada. The spatial and temporal pattern of the highest retrieved CHO.CHO and HCHO VCDs are associated with areas having high fire radiative power, as identified in the MODIS fire data products. This indicates that in these areas, pyrogenic emissions are the dominant source of CHO.CHO and HCHO. In

addition to local enhancements of NO_2, CHO.CHO, and HCHO, close to the fires, extended plumes of elevated CHO.CHO and HCHO VCD are observed downwind from the fires. This is in contrast with the behaviour of NO_2, which is also transported but is short lived. The spatial and temporal CHO.CHO and HCHO distribution observed from satellite follows a similar pattern to that of CO, which is long lived, and that simulated by the FLEXPART dispersion model, initialized by tracer emissions starting at known fire locations. Enhanced CHO.CHO and HCHO were found in the S5P data up to 1500 km from their sources.

In order to obtain reasonable agreement between the model results and the measurements, an effective tracer lifetime of more than 20 hours and up to 28.9 hours needs to be assumed in the FLEXPART simulations. This is significantly longer than the anticipated lifetimes of CHO.CHO and HCHO. The transport of CHO.CHO and HCHO along the length of the plume could be associated with these trace gases being lifted from the boundary layer into the free troposphere, where high wind speeds lead to rapid transport. The long apparent lifetime of CHO.CHO and HCHO in the transported plumes could be explained by a real increase in their lifetime in the plume because of photochemical conditions in the plume, which we consider unexpected. Based on our current knowledge, the most probable explanation of the apparent long lifetime of CHO.CHO and HCHO would be formation within the plume caused by the oxidation of a mixture of longer-lived emitted VOC precursors (e.g. methanol, ethanol, acetylene, aromatics, glycolaldehyde, ethylene etc.), that form CHO.CHO and HCHO at different rates. Further research is needed to investigate how frequent such fire-related long-range transport events of VOCs are. The chemical mechanism of the formation of the CHO.CHO and HCHO in the plumes downwind of the fires needs to be identified. The assessment of the number of such fires events and their relevance for tropospheric O_3 and aerosol production downwind of the fires and air quality is required.

Data availability. The Global Fire Assimilation System are available in the database of The Copernicus Atmosphere Monitoring Service (https://apps.ecmwf.int/, last access: 7 November 2018). The CALIPSO: Cloud and Aerosol Lidar Level 2 Aerosol Profile Version 3-02 Product (CAL_LID_L2_05kmAPro-Prov-V3-02) are available at the NASA Langley Research Center Atmospheric Science Data Center DAAC (https://eosweb.larc.nasa.gov/, last access: 29 March 2019). The Suomi NPP Visible Infrared Imaging Radiometer Suite (VIIRS) true colour images are available at the NASA Langley Research Center Atmospheric Science Data Center DAAC (https://wvs.earthdata.nasa.gov/, last access: 19 June 2019). The FLEXPART simulations, Level 2 and Level 3 CHOCHO and HCHO data are available at Institute of Environmental Physics of University of Bremen (http://www.iup.uni-bremen.de/doas/data/glyoxal/S5P/alvarado_2020/).

Author contributions. L. M. A. Alvarado, A. Richter and J. P. Burrows have prepared the manuscript with the contribution of all authors and developed the glyoxal and formaldehyde and NO_2 retrievals for TROPOMI measurements. M. Vrekoussis, A. Hilboll and A. B. Kalisz Hedegaard have designed and performed the FLEXPART simulations of the airmasses assuming

different effective lifetimes. O. Schneising has developed the CO retrieval and provided the CO data for the comparison with glyoxal and formaldehyde products.

Competing interests. The authors declare that they have no conflict of interest.

Acknowledgements. The authors acknowledge financial support provided by the University of Bremen. Copernicus Sentinel-5P lv1 data from 2018 were used in this study. This publication contains modified COPERNICUS Sentinel data (2018). We thank the MACC team for providing the GFASv1.0 FRP and injection height products. FLEXPART simulations were conducted on the University of Bremen's HPC cluster Aether, funded by DFG within the scope of the Excellence Initiative. VIIRS and CALIPSO data were obtained from the NASA Langley Research Center Atmospheric Science Data Center. FLEXPART simulation results were generated using Copernicus Climate Change Service Information (ERA5).

This is in part preparatory work for the analysis of the data from the DFG SPP HALO EMeRGe project, which has one focus on biomass burning and the long range transport of such plumes. We thank Abram Sanders (European Organisation for the Exploitation of Meteorological Satellites, Darmstadt) for providing support in the preparation of CALIPSO data for the computation of CHO.CHO and HCHO AMFs.

References

Abbot, D. S., Palmer, P. I., Martin, R. V., Chance, K. V., Jacob, D. J. and Guenther, A.: Seasonal and interannual variability of North American isoprene emissions as determined by formaldehyde column measurements from space, Geophysical Research Letters, 30(17), doi:10.1029/2003GL017336, 2003.

Alvarado, L. M. A.: Investigating the role of glyoxal using satellite and MAX-DOAS measurements, PhD, University of Bremen., 2016.

Alvarado, L. M. A., Richter, A., Vrekoussis, M., Wittrock, F., Hilboll, A., Schreier, S. F. and Burrows, J. P.: An improved glyoxal retrieval from OMI measurements, Atmos. Meas. Tech., 7(12), 4133–4150, doi:10.5194/amt-7-4133-2014, 2014.

Alvarado, L. M. A., Richter, A., Vrekoussis, M., Wittrock, F., Hilboll, A., Schreier, S. F. and Burrows, J. P.: Investigating the Link Between Glyoxal and Biogenic Activities, in Towards an Interdisciplinary Approach in Earth System Science,

edited by G. Lohmann, H. Meggers, V. Unnithan, D. Wolf-Gladrow, J. Notholt, and A. Bracher, pp. 59–65, Springer International Publishing., 2015.

Atkinson, R.: Atmospheric chemistry of VOCs and NOx, Atmospheric Environment, 34(12–14), 2063–2101, doi:10.1016/S1352-2310(99)00460-4, 2000.

Behrens, L. K., Hilboll, A., Richter, A., Peters, E., Alvarado, L. M. A., Kalisz Hedegaard, A. B., Wittrock, F., Burrows, J. P. and Vrekoussis, M.: Detection of outflow of formaldehyde and glyoxal from the African continent to the Atlantic Ocean with a MAX-DOAS instrument, Atmospheric Chemistry and Physics, 19(15), 10257–10278, doi:https://doi.org/10.5194/acp-19-10257-2019, 2019.

Bovensmann, H., Burrows, J. P., Buchwitz, M., Frerick, J., Noël, S., Rozanov, V. V., Chance, K. V. and Goede, A. P. H.: SCIAMACHY: Mission Objectives and Measurement Modes, Journal of the Atmospheric Sciences, 56(2), 127–150, doi:10.1175/1520-0469(1999)056<0127:SMOAMM>2.0.CO;2, 1999.

Burrows, J. P., Hölzle, E., Goede, A. P. H., Visser, H. and Fricke, W.: SCIAMACHY—scanning imaging absorption spectrometer for atmospheric chartography, Acta Astronautica, 35(7), 445–451, doi:10.1016/0094-5765(94)00278-T, 1995.

Burrows, J. P., Weber, M., Buchwitz, M., Rozanov, V., Ladstätter-Weißenmayer, A., Richter, A., DeBeek, R., Hoogen, R., Bramstedt, K., Eichmann, K.-U., Eisinger, M. and Perner, D.: The Global Ozone Monitoring Experiment (GOME): Mission Concept and First Scientific Results, Journal of the Atmospheric Sciences, 56(2), 151–175, doi:10.1175/1520-0469(1999)056<0151:TGOMEG>2.0.CO;2, 1999.

Chan Miller, C., Gonzalez Abad, G., Wang, H., Liu, X., Kurosu, T., Jacob, D. J. and Chance, K.: Glyoxal retrieval from the Ozone Monitoring Instrument, Atmos. Meas. Tech., 7(11), 3891–3907, doi:10.5194/amt-7-3891-2014, 2014.

De Smedt, I., Müller, J.-F., Stavrakou, T., van der A, R., Eskes, H. and Van Roozendael, M.: Twelve years of global observations of formaldehyde in the troposphere using GOME and SCIAMACHY sensors, Atmos. Chem. Phys., 8(16), 4947–4963, doi:10.5194/acp-8-4947-2008, 2008.

De Smedt, I., Van Roozendael, M., Stavrakou, T., Müller, J.-F., Lerot, C., Theys, N., Valks, P., Hao, N. and van der A, R.: Improved retrieval of global tropospheric formaldehyde columns from GOME-2/MetOp-A addressing noise reduction and instrumental degradation issues, Atmos. Meas. Tech., 5(11), 2933–2949, doi:10.5194/amt-5-2933-2012, 2012.

De Smedt, I., Stavrakou, T., Hendrick, F., Danckaert, T., Vlemmix, T., Pinardi, G., Theys, N., Lerot, C., Gielen, C., Vigouroux, C., Hermans, C., Fayt, C., Veefkind, P., Müller, J.-F. and Van Roozendael, M.: Diurnal, seasonal and long-term variations of global formaldehyde columns inferred from combined OMI and GOME-2 observations, Atmos. Chem. Phys., 15(21), 12519–12545, doi:10.5194/acp-15-12519-2015, 2015.

De Smedt, I., Theys, N., Yu, H., Danckaert, T., Lerot, C., Compernolle, S., Roozendael, M. V., Richter, A., Hilboll, A., Peters, E., Pedergnana, M., Loyola, D., Beirle, S., Wagner, T., Eskes, H., Geffen, J. van, Boersma, K. F. and Veefkind, P.: Algorithm theoretical baseline for formaldehyde retrievals from S5P TROPOMI and from the QA4ECV project, Atmospheric Measurement Techniques, 11(4), 2395–2426, doi:https://doi.org/10.5194/amt-11-2395-2018, 2018.

Fleischmann, O. C., Hartmann, M., Burrows, J. P. and Orphal, J.: New ultraviolet absorption cross-sections of BrO at atmospheric temperatures measured by time-windowing Fourier transform spectroscopy, Journal of Photochemistry and Photobiology A: Chemistry, 168(1–2), 117–132, doi:10.1016/j.jphotochem.2004.03.026, 2004.

Folkins, I., Wennberg, P. O., Hanisco, T. F., Anderson, J. G. and Salawitch, R. J.: OH, HO2, and NO in two biomass burning plumes: Sources of HOx and implications for ozone production, Geophysical Research Letters, 24(24), 3185–3188, doi:10.1029/97GL03047, 1997.

Fu, T.-M., Jacob, D. J., Palmer, P. I., Chance, K., Wang, Y. X., Barletta, B., Blake, D. R., Stanton, J. C. and Pilling, M. J.: Space-based formaldehyde measurements as constraints on volatile organic compound emissions in east and south Asia and implications for ozone, Journal of Geophysical Research: Atmospheres, 112(D6), n/a–n/a, doi:10.1029/2006JD007853, 2007.

González Abad, G., Liu, X., Chance, K., Wang, H., Kurosu, T. P. and Suleiman, R.: Updated Smithsonian Astrophysical Observatory Ozone Monitoring Instrument (SAO OMI) formaldehyde retrieval, Atmos. Meas. Tech., 8(1), 19–32, doi:10.5194/amt-8-19-2015, 2015.

Guenther, A., Geron, C., Pierce, T., Lamb, B., Harley, P. and Fall, R.: Natural emissions of non-methane volatile organic compounds, carbon monoxide, and oxides of nitrogen from North America, Atmospheric Environment, 34(12–14), 2205–2230, doi:10.1016/S1352-2310(99)00465-3, 2000.

Guenther, A., Karl, T., Harley, P., Wiedinmyer, C., Palmer, P. I. and Geron, C.: Estimates of global terrestrial isoprene emissions using MEGAN (Model of Emissions of Gases and Aerosols from Nature), Atmos. Chem. Phys., 6(11), 3181–3210, doi:10.5194/acp-6-3181-2006, 2006.

Hewson, W., Bösch, H., Barkley, M. P. and De Smedt, I.: Characterisation of GOME-2 formaldehyde retrieval sensitivity, Atmos. Meas. Tech., 6(2), 371–386, doi:10.5194/amt-6-371-2013, 2013.

Jang, M., Czoschke, N. M., Lee, S. and Kamens, R. M.: Heterogeneous Atmospheric Aerosol Production by Acid-Catalyzed Particle-Phase Reactions, Science, 298(5594), 814–817, doi:10.1126/science.1075798, 2002.

Justice, C. O., Giglio, L., Korontzi, S., Owens, J., Morisette, J. T., Roy, D., Descloitres, J., Alleaume, S., Petitcolin, F. and

Kaufman, Y.: The MODIS fire products, Remote Sensing of Environment, 83(1–2), 244–262, doi:10.1016/S0034-4257(02)00076-7, 2002.

Kaiser, J. W., Heil, A., Andreae, M. O., Benedetti, A., Chubarova, N., Jones, L., Morcrette, J.-J., Razinger, M., Schultz, M. G., Suttie, M. and van der Werf, G. R.: Biomass burning emissions estimated with a global fire assimilation system based on observed fire radiative power, Biogeosciences, 9(1), 527–554, doi:10.5194/bg-9-527-2012, 2012.

Kansal, A.: Sources and reactivity of NMHCs and VOCs in the atmosphere: A review, Journal of Hazardous Materials, 166(1), 17–26, doi:10.1016/j.jhazmat.2008.11.048, 2009.

Kroll, J. H., Ng, N. L., Murphy, S. M., Varutbangkul, V., Flagan, R. C. and Seinfeld, J. H.: Chamber studies of secondary organic aerosol growth by reactive uptake of simple carbonyl compounds, J. Geophys. Res., 110(D23), D23207, doi:10.1029/2005JD006004, 2005.

Kurosu, T. P., Chance, K. and Volkamer, R.: Measurements of HCHO, CHOCHO, and BrO from the Ozone Monitoring Instrument on EOS AURA, in Proceedings of Envisat Symposium., 2007.

Lerot, C., Stavrakou, T., De Smedt, I., Müller, J.-F. and Van Roozendael, M.: Glyoxal vertical columns from GOME-2 backscattered light measurements and comparisons with a global model, Atmos. Chem. Phys., 10(24), 12059–12072, doi:10.5194/acp-10-12059-2010, 2010.

Levelt, P. F., van den Oord, G. H. J., Dobber, M. R., Malkki, A., Visser, H., Vries, J. de, Stammes, P., Lundell, J. O. V. and Saari, H.: The ozone monitoring instrument, IEEE Transactions on Geoscience and Remote Sensing, 44(5), 1093 – 1101, doi:10.1109/TGRS.2006.872333, 2006.

Liggio, J., Li, S.-M. and McLaren, R.: Reactive uptake of glyoxal by particulate matter, Journal of Geophysical Research: Atmospheres, 110(D10), doi:10.1029/2004JD005113, 2005.

Liu, Z., Wang, Y., Vrekoussis, M., Richter, A., Wittrock, F., Burrows, J. P., Shao, M., Chang, C.-C., Liu, S.-C., Wang, H. and Chen, C.: Exploring the missing source of glyoxal (CHOCHO) over China, Geophysical Research Letters, 39(10), doi:10.1029/2012GL051645, 2012.

Loeffler, K. W., Koehler, C. A., Paul, N. M. and De Haan, D. O.: Oligomer Formation in Evaporating Aqueous Glyoxal and Methyl Glyoxal Solutions, Environ. Sci. Technol., 40(20), 6318–6323, doi:10.1021/es060810w, 2006.

Marais, E. A., Jacob, D. J., Kurosu, T. P., Chance, K., Murphy, J. G., Reeves, C., Mills, G., Casadio, S., Millet, D. B., Barkley, M. P., Paulot, F. and Mao, J.: Isoprene emissions in Africa inferred from OMI observations of formaldehyde columns, Atmos. Chem. Phys., 12(14), 6219–6235, doi:10.5194/acp-12-6219-2012, 2012.

Mason, J. D., Cone, M. T. and Fry, E. S.: Ultraviolet (250–550 nm) absorption spectrum of pure water, Appl. Opt., AO, 55(25), 7163–7172, doi:10.1364/AO.55.007163, 2016.

Meller, R. and Moortgat, G. K.: Temperature dependence of the absorption cross sections of formaldehyde between 223 and 323 K in the wavelength range 225–375 nm, J. Geophys. Res., 105(D6), 7089–7101, doi:10.1029/1999JD901074, 2000.

Munro, R., Lang, R., Klaes, D., Poli, G., Retscher, C., Lindstrot, R., Huckle, R., Lacan, A., Grzegorski, M., Holdak, A., Kokhanovsky, A., Livschitz, J. and Eisinger, M.: The GOME-2 instrument on the Metop series of satellites: instrument design, calibration, and level 1 data processing – an overview, Atmos. Meas. Tech., 9(3), 1279–1301, doi:10.5194/amt-9-1279-2016, 2016.

Myriokefalitakis, S., Vrekoussis, M., Tsigaridis, K., Wittrock, F., Richter, A., Brühl, C., Volkamer, R., Burrows, J. P. and Kanakidou, M.: The influence of natural and anthropogenic secondary sources on the glyoxal global distribution, Atmos. Chem. Phys., 8(16), 4965–4981, doi:10.5194/acp-8-4965-2008, 2008.

Natural Resources Canada: Canadian Wildland Fire Information System | Archived reports, [online] Available from: http://cwfis.cfs.nrcan.gc.ca/report/archives?year=2018&month=08&day=29&process=Submit (Accessed 12 April 2019), 2018.

Palmer, P. I., Jacob, D. J., Chance, K., Martin, R. V., Spurr, R. J. D., Kurosu, T. P., Bey, I., Yantosca, R., Fiore, A. and Li, Q.: Air mass factor formulation for spectroscopic measurements from satellites: Application to formaldehyde retrievals from the Global Ozone Monitoring Experiment, Journal of Geophysical Research: Atmospheres, 106(D13), 14539–14550, doi:10.1029/2000JD900772, 2001.

Palmer, P. I., Jacob, D. J., Fiore, A. M., Martin, R. V., Chance, K. and Kurosu, T. P.: Mapping isoprene emissions over North America using formaldehyde column observations from space, Journal of Geophysical Research: Atmospheres, 108(D6), n/a–n/a, doi:10.1029/2002JD002153, 2003.

Pisso, I., Sollum, E., Grythe, H., Kristiansen, N., Cassiani, M., Eckhardt, S., Arnold, D., Morton, D., Thompson, R. L., Groot Zwaaftink, C. D., Evangeliou, N., Sodemann, H., Haimberger, L., Henne, S., Brunner, D., Burkhart, J. F., Fouilloux, A., Brioude, J., Philipp, A., Seibert, P. and Stohl, A.: The Lagrangian particle dispersion model FLEXPART version 10.3, Geoscientific Model Development Discussions, 1–67, doi:https://doi.org/10.5194/gmd-2018-333, 2019.

Puķīte, J., Kühl, S., Deutschmann, T., Platt, U. and Wagner, T.: Extending differential optical absorption spectroscopy for limb measurements in the UV, Atmos. Meas. Tech., 3(3), 631–653, doi:10.5194/amt-3-631-2010, 2010.

Rémy, S., Veira, A., Paugam, R., Sofiev, M., Kaiser, J. W., Marenco, F., Burton, S. P., Benedetti, A., Engelen, R. J., Ferrare, R. and Hair, J. W.: Two global data sets of daily fire emission injection heights since 2003, Atmospheric Chemistry and Physics, 17(4), 2921–2942, doi:https://doi.org/10.5194/acp-17-2921-2017, 2017.

Richter, A., Begoin, M., Hilboll, A. and Burrows, J. P.: An improved NO2 retrieval for the GOME-2 satellite instrument, Atmos. Meas. Tech., 4(6), 1147–1159, doi:10.5194/amt-4-1147-2011, 2011.

Rothman, L. S., Gordon, I. E., Babikov, Y., Barbe, A., Chris Benner, D., Bernath, P. F., Birk, M., Bizzocchi, L., Boudon, V., Brown, L. R., Campargue, A., Chance, K., Cohen, E. A., Coudert, L. H., Devi, V. M., Drouin, B. J., Fayt, A., Flaud, J.-M., Gamache, R. R., Harrison, J. J., Hartmann, J.-M., Hill, C., Hodges, J. T., Jacquemart, D., Jolly, A., Lamouroux, J., Le Roy, R. J., Li, G., Long, D. A., Lyulin, O. M., Mackie, C. J., Massie, S. T., Mikhailenko, S., Müller, H. S. P., Naumenko, O. V., Nikitin, A. V., Orphal, J., Perevalov, V., Perrin, A., Polovtseva, E. R., Richard, C., Smith, M. A. H., Starikova, E., Sung, K., Tashkun, S., Tennyson, J., Toon, G. C., Tyuterev, Vl. G. and Wagner, G.: The HITRAN2012 molecular spectroscopic database, Journal of Quantitative Spectroscopy and Radiative Transfer, 130, 4–50, doi:10.1016/j.jqsrt.2013.07.002, 2013.

Rozanov, V. V., Rozanov, A. V., Kokhanovsky, A. A. and Burrows, J. P.: Radiative transfer through terrestrial atmosphere and ocean: Software package SCIATRAN, Journal of Quantitative Spectroscopy and Radiative Transfer, doi:10.1016/j.jqsrt.2013.07.004, 2013.

Schneising, O., Buchwitz, M., Reuter, M., Bovensmann, H., Burrows, J. P., Borsdorff, T., Deutscher, N. M., Feist, D. G., Griffith, D. W. T., Hase, F., Hermans, C., Iraci, L. T., Kivi, R., Landgraf, J., Morino, I., Notholt, J., Petri, C., Pollard, D. F., Roche, S., Shiomi, K., Strong, K., Sussmann, R., Velazco, V. A., Warneke, T. and Wunch, D.: A scientific algorithm to simultaneously retrieve carbon monoxide and methane from TROPOMI onboard Sentinel-5 Precursor, Atmospheric Measurement Techniques Discussions, 1–44, doi:https://doi.org/10.5194/amt-2019-243, 2019.

Schweitzer, F., Magi, L., Mirabel, P. and George, C.: Uptake Rate Measurements of Methanesulfonic Acid and Glyoxal by Aqueous Droplets, J. Phys. Chem. A, 102(3), 593–600, doi:10.1021/jp972451k, 1998.

Serdyuchenko, A., Gorshelev, V., Weber, M., Chehade, W. and Burrows, J. P.: High spectral resolution ozone absorption cross-sections – Part 2: Temperature dependence, Atmospheric Measurement Techniques, 7(2), 625–636, doi:https://doi.org/10.5194/amt-7-625-2014, 2014.

Sinreich, R., Volkamer, R., Filsinger, F., Frieß, U., Kern, C., Platt, U., Sebastián, O. and Wagner, T.: MAX-DOAS detection of glyoxal during ICARTT 2004, Atmos. Chem. Phys., 7(5), 1293–1303, doi:10.5194/acp-7-1293-2007, 2007.

Sinreich, R., Coburn, S., Dix, B. and Volkamer, R.: Ship-based detection of glyoxal over the remote tropical Pacific Ocean, Atmos. Chem. Phys., 10(23), 11359–11371, doi:10.5194/acp-10-11359-2010, 2010.

Stavrakou, T., Müller, J.-F., De Smedt, I., Van Roozendael, M., van der Werf, G. R., Giglio, L. and Guenther, A.: Evaluating the performance of pyrogenic and biogenic emission inventories against one decade of space-based formaldehyde columns, Atmos. Chem. Phys., 9(3), 1037–1060, doi:10.5194/acp-9-1037-2009, 2009a.

Stavrakou, T., Müller, J.-F., De Smedt, I., Van Roozendael, M., van der Werf, G. R., Giglio, L. and Guenther, A.: Global emissions of non-methane hydrocarbons deduced from SCIAMACHY formaldehyde columns through 2003–2006, Atmos. Chem. Phys., 9(11), 3663–3679, doi:10.5194/acp-9-3663-2009, 2009b.

Stavrakou, T., Müller, J.-F., De Smedt, I., Van Roozendael, M., Kanakidou, M., Vrekoussis, M., Wittrock, F., Richter, A. and Burrows, J. P.: The continental source of glyoxal estimated by the synergistic use of spaceborne measurements and inverse modelling, Atmos. Chem. Phys., 9(21), 8431–8446, doi:10.5194/acp-9-8431-2009, 2009c.

Stohl, A., Forster, C., Frank, A., Seibert, P. and Wotawa, G.: Technical note: The Lagrangian particle dispersion model FLEXPART version 6.2, Atmospheric Chemistry and Physics, 5(9), 2461–2474, doi:https://doi.org/10.5194/acp-5-2461-2005, 2005.

Thalman, R., Baeza-Romero, M. T., Ball, S. M., Borrás, E., Daniels, M. J. S., Goodall, I. C. A., Henry, S. B., Karl, T., Keutsch, F. N., Kim, S., Mak, J., Monks, P. S., Muñoz, A., Orlando, J., Peppe, S., Rickard, A. R., Ródenas, M., Sánchez, P., Seco, R., Su, L., Tyndall, G., Vázquez, M., Vera, T., Waxman, E. and Volkamer, R.: Instrument intercomparison of glyoxal, methyl glyoxal and NO2 under simulated atmospheric conditions, Atmos. Meas. Tech., 8(4), 1835–1862, doi:10.5194/amt-8-1835-2015, 2015.

Urbanski, S. P., Reeves, M. C., Corley, R. E., Silverstein, R. P. and Hao, W. M.: Contiguous United States wildland fire emission estimates during 2003–2015, Earth System Science Data, 10(4), 2241–2274, doi:https://doi.org/10.5194/essd-10-2241-2018, 2018.

Vandaele, A. C., Hermans, C., Simon, P. C., Carleer, M., Colin, R., Fally, S., Mérienne, M. F., Jenouvrier, A. and Coquart, B.: Measurements of the NO_2 absorption cross-section from 42000 cm-1 to 10000 cm-1 (238-1000 nm) at 220 K and 294 K, Journal of Quantitative Spectroscopy and Radiative Transfer, 59(3–5), 171–184, doi:10.1016/S0022-4073(97)00168-4, 1998.

Vaughan, M. A., Young, S. A., Winker, D. M., Powell, K. A., Omar, A. H., Liu, Z., Hu, Y. and Hostetler, C. A.: Fully automated analysis of space-based lidar data: an overview of the CALIPSO retrieval algorithms and data products, in Laser Radar Techniques for Atmospheric Sensing, vol. 5575, pp. 16–30, International Society for Optics and Photonics., 2004.

Veefkind, J. P., Aben, I., McMullan, K., Förster, H., de Vries, J., Otter, G., Claas, J., Eskes, H. J., de Haan, J. F., Kleipool, Q., van Weele, M., Hasekamp, O., Hoogeveen, R., Landgraf, J., Snel, R., Tol, P., Ingmann, P., Voors, R., Kruizinga, B., Vink, R., Visser, H. and Levelt, P. F.: TROPOMI on the ESA Sentinel-5 Precursor: A GMES mission for global observations of the atmospheric composition for climate, air quality and ozone layer applications, Remote Sensing of Environment, 120, 70–83, doi:10.1016/j.rse.2011.09.027, 2012.

Volkamer, R., Molina, L. T., Molina, M. J., Shirley, T. and Brune, W. H.: DOAS measurement of glyoxal as an indicator for fast VOC chemistry in urban air, Geophysical Research Letters, 32(8), n/a–n/a, doi:10.1029/2005GL022616, 2005a.

Volkamer, R., Spietz, P., Burrows, J. and Platt, U.: High-resolution absorption cross-section of glyoxal in the UV–vis and IR spectral ranges, Journal of Photochemistry and Photobiology A: Chemistry, 172(1), 35–46, doi:10.1016/j.jphotochem.2004.11.011, 2005b.

Volkamer, R., San Martini, F., Molina, L. T., Salcedo, D., Jimenez, J. L. and Molina, M. J.: A missing sink for gas-phase glyoxal in Mexico City: Formation of secondary organic aerosol, Geophysical Research Letters, 34(19), doi:10.1029/2007GL030752, 2007.

Vountas, M., Rozanov, V. V. and Burrows, J. P.: Ring effect: Impact of rotational Raman scattering on radiative transfer in earth's atmosphere, Journal of Quantitative Spectroscopy and Radiative Transfer, 60(6), 943–961, doi:10.1016/S0022-4073(97)00186-6, 1998.

Vrekoussis, M., Wittrock, F., Richter, A. and Burrows, J. P.: Temporal and spatial variability of glyoxal as observed from space, Atmos. Chem. Phys., 9(13), 4485–4504, doi:10.5194/acp-9-4485-2009, 2009.

Vrekoussis, M., Wittrock, F., Richter, A. and Burrows, J. P.: GOME-2 observations of oxygenated VOCs: what can we learn from the ratio glyoxal to formaldehyde on a global scale?, Atmos. Chem. Phys., 10(21), 10145–10160, doi:10.5194/acp-10-10145-2010, 2010.

Wittrock, F., Richter, A., Oetjen, H., Burrows, J. P., Kanakidou, M., Myriokefalitakis, S., Volkamer, R., Beirle, S., Platt, U. and Wagner, T.: Simultaneous global observations of glyoxal and formaldehyde from space, Geophysical Research Letters, 33(16), n/a–n/a, doi:10.1029/2006GL026310, 2006.

690 Zhang, Y., Wang, X., Wen, S., Herrmann, H., Yang, W., Huang, X., Zhang, Z., Huang, Z., He, Q. and George, C.: On-road vehicle emissions of glyoxal and methylglyoxal from tunnel tests in urban Guangzhou, China, Atmospheric Environment, 127, 55–60, doi:10.1016/j.atmosenv.2015.12.017, 2016.

Zien, A. W., Richter, A., Hilboll, A., Blechschmidt, A.-M. and Burrows, J. P.: Systematic analysis of tropospheric NO2
695 long-range transport events detected in GOME-2 satellite data, Atmos. Chem. Phys., 14(14), 7367–7396, doi:10.5194/acp-14-7367-2014, 2014.